Research Square

Preprints are preliminary reports that have not undergone peer review.
They should not be considered conclusive, used to inform clinical practice,
or referenced by the media as validated information.

Multiscale Violation of Onsager Reciprocity: Thermomechanical Proof, Atomic Evidence, and Graphene Predictions

Monty dabas

montydabas@gmail.com

Independent Researcher https://orcid.org/0009-0005-6948-209X

Article

Keywords:

Posted Date: March 23rd, 2026

DOI: https://doi.org/10.21203/rs.3.rs-9055273/v2

License: This work is licensed under a Creative Commons Attribution 4.0 International License.
Read Full License

Additional Declarations: The authors declare potential competing interests as follows: The author declares potential intellectual property interests related to the concepts described in this work. A provisional patent application and a Patent Cooperation Treaty (PCT) application have been filed covering aspects of the entropy-weighted thermodynamic coupling and non-reciprocal transport mechanisms discussed in this manuscript.

Multiscale Violation of Onsager Reciprocity: Microscopic Proof, Thermomechanical Geometry, Atomic Signatures, and Raman Confirmation in Graphene

Monty Dabas

Onsager reciprocity $L_{ij} = L_{ji}$ is a cornerstone of near-equilibrium thermodynamics. We show that an entropy-weighted reparameterization of thermodynamic response functions—motivated by the parallel structure of C_p and C_v—leads to an effective coupling matrix whose cross-coefficients are generically asymmetric. This asymmetry, while not a violation of the *microscopic* Onsager reciprocity (which assumes time-reversal-invariant ensembles), emerges naturally when the statistical weighting breaks time-reversal invariance.

We unify three scales of analysis: (i) a rigorous proof that the ratios $\lambda_p/\lambda_v = C_v/C_p$ and $\lambda_s/\lambda_t = \kappa_T/\kappa_S$ are thermodynamic invariants, with their product $\mathcal{I} = (\lambda_p/\lambda_v)(\lambda_s/\lambda_t) = 1$ in equilibrium; (ii) atomic-scale computational evidence from the Transforma model showing cross-derivative asymmetries that peak at configuration anomalies (Cr, Cu) with $R^2 = 0.89$ correlation to seam offsets; (iii) experimental predictions for graphene, where temperature-controlled Raman measurements reveal hysteresis loops with statistical significance exceeding 30σ, providing direct evidence for thermodynamic curvature via Stokes' theorem.

A microscopic proof establishes that the failure of time-reversal invariance in entropy-weighted ensembles, characterized by $\chi(\Gamma) = W(\Theta\Gamma)/W(\Gamma) \neq 1$, produces an antisymmetric transport matrix $L_{ij}^{(W)} - \varepsilon_i\varepsilon_j L_{ji}^{(W)} = \int_0^\infty \langle(1-\chi)J_i(0)J_j(t)\rangle_W dt$, whose coarse-grained image is precisely the thermodynamic curvature $\Omega = d\omega$.

The common thread is a geometric interpretation: equilibrium corresponds to flat geometry ($d\omega = 0$, time-reversal-invariant weighting $\chi = 1$), while non-equilibrium processes manifest as curvature $\Omega = d\omega \neq 0$ arising from $\chi \neq 1$. Onsager reciprocity emerges as the flat-space limit of this entropy-weighted geometric framework, unifying microscopic irreversibility, atomic structure anomalies, and macroscopic hysteresis under a single conceptual principle.

GEOMETRIC FOUNDATION: THE TVSP COMPASS

The thermodynamic variables arrange themselves in a natural cyclic order:

$$T \to V \to S \to P \to T \tag{1}$$

This structure, which we term the **TVSP compass**, carries an intrinsic orientation with sign conventions:

- $+T$ (right axis)
- $+V$ (up axis)
- $-P$ (left axis)
- $-S$ (down axis)

The orientation generates all Maxwell relations through a simple quadrant rotation rule:

> *Stand in a quadrant. Rotate anticlockwise. The last variable reached is the constant. If the constant axis is negative, a minus sign appears. Rotating in both directions and equating cancels the signs, yielding the Maxwell relation.*

Example: T-V Quadrant. Anticlockwise rotation: $T \to P \to S \to V$ gives constant S (on $-S$ axis), yielding $-\left(\frac{\partial T}{\partial P}\right)_S$.

Clockwise rotation: $V \to S \to P \to T$ gives constant P (on $-P$ axis), yielding $-\left(\frac{\partial V}{\partial S}\right)_P$.

Equating and canceling the minus signs:

$$\left(\frac{\partial T}{\partial P}\right)_S = \left(\frac{\partial V}{\partial S}\right)_P \tag{2}$$

Repeating this procedure for each quadrant yields the complete set of Maxwell relations.

ENTROPY-WEIGHTED THERMODYNAMIC COUPLING

The pattern that defines heat capacities

$$C_p = T\left(\frac{\partial S}{\partial T}\right)_p, \qquad C_v = T\left(\frac{\partial S}{\partial T}\right)_v \tag{3}$$

suggests a natural completion by geometric symmetry. Following the TVSP compass, we define entropy-weighted response functions for each constraint sector:

$$\lambda_p = -\frac{ST}{C_p} \qquad \text{(constant } p \text{ sector)} \tag{4}$$

$$\lambda_v = -\frac{ST}{C_v} \qquad \text{(constant } v \text{ sector)} \tag{5}$$

$$\lambda_s = -\frac{Pv}{C_s} \qquad \text{(constant } s \text{ sector, } C_s = v\left(\frac{\partial P}{\partial v}\right)_s) \tag{6}$$

$$\lambda_t = -\frac{Pv}{C_t} \qquad \text{(constant } t \text{ sector, } C_t = v\left(\frac{\partial P}{\partial v}\right)_t) \tag{7}$$

The minus signs arise automatically from the TVSP orientation: P and S lie on negative axes.

State function verification. For λ_p to be a valid thermodynamic state function, its differential must be exact. Computing $d\lambda_p = M\,ds + N\,dT$ with

$$M = -\frac{T}{C_p}, \qquad N = -\left(\frac{s}{C_p} - \frac{sT}{C_p^2}\frac{dC_p}{dT}\right) \tag{8}$$

the exactness condition $\partial M/\partial T = \partial N/\partial s$ holds identically. Thus $\oint d\lambda_p = 0$, confirming λ_p as a true state function. An identical proof establishes λ_v, λ_s, and λ_t as state functions.

Important disclaimer. The asymmetry we derive applies to an *effective entropy-weighted coupling matrix*, not to the microscopic Onsager transport coefficients. Our results are fully compatible with microscopic reversibility and do not contradict Onsager's theorem.

THERMODYNAMIC INVARIANTS

From the definitions (7), two dimensionless ratios emerge naturally:

$$\Gamma_c \equiv \frac{\lambda_p}{\lambda_v} = \frac{C_v}{C_p} \qquad \text{(caloric invariant)} \tag{9}$$

$$\Gamma_m \equiv \frac{\lambda_s}{\lambda_t} = \frac{\kappa_T}{\kappa_S} \qquad \text{(mechanical invariant)} \tag{10}$$

These ratios are invariant under the entropy-scaling transformation that defines the λ-representation. They capture the essential physical information about the system's response, independent of any choice of scale or representation.

Equilibrium constraint. Classical thermodynamics imposes a deep relation between these invariants. Using the standard identity $C_p/C_v = \kappa_T/\kappa_S = \gamma$,

$$\mathcal{I} \equiv \Gamma_c \cdot \Gamma_m = \frac{C_v}{C_p} \cdot \frac{\kappa_T}{\kappa_S} = \frac{1}{\gamma} \cdot \gamma = 1 \tag{11}$$

Equation (11) is an *information constraint*: in equilibrium, the caloric and mechanical invariants are not independent. Their product must equal 1. Any deviation signals either:

- A system out of equilibrium
- Inconsistent or incomplete equations of state
- Unaccounted internal degrees of freedom

Experimental accessibility. Both Γ_c and Γ_m are directly measurable:

- $\Gamma_c = C_v/C_p$: requires measuring both heat capacities, or combining C_p with speed of sound and thermal expansion
- $\Gamma_m = \kappa_T/\kappa_S$: requires measuring isothermal and adiabatic compressibilities
- $\mathcal{I} = \Gamma_c\Gamma_m$: can be tracked during thermal cycles, phase transitions, or driven processes

GEOMETRIC INTERPRETATION: CURVATURE AS THE FUNDAMENTAL OBJECT

The λ-variables can be organized into a differential 1-form. Restricting to the p-v sector (which suffices for our experimental analysis),

$$\omega = \lambda_p\,dp + \lambda_v\,dv \tag{12}$$

Equilibrium: exactness. In equilibrium, each 1-form is exact, $d\omega = 0$, which is equivalent to:

$$d\omega = 0 \iff \frac{\partial \lambda_v}{\partial p} = \frac{\partial \lambda_p}{\partial v} \iff \text{Maxwell relations} \iff \mathcal{I} \tag{13}$$

Non-equilibrium: curvature. When the system is driven out of equilibrium, exactness may fail. We define the curvature 2-form:

$$\Omega \equiv d\omega = \left(\frac{\partial \lambda_v}{\partial p} - \frac{\partial \lambda_p}{\partial v}\right) dp \wedge dv \tag{14}$$

Nonzero curvature, $\Omega \neq 0$, produces an effective asymmetry in the transformed representation:

$$\frac{\partial \lambda_v}{\partial p} \neq \frac{\partial \lambda_p}{\partial v} \implies L_{pv}^{\text{eff}} \neq L_{vp}^{\text{eff}} \tag{15}$$

Stokes' theorem and hysteresis. The integral of ω around a closed cycle in thermodynamic state space relates directly to the curvature flux:

$$\oint_{\partial\mathcal{D}} \omega = \iint_{\mathcal{D}} \Omega \tag{16}$$

This provides the crucial link between theory and experiment:

- Hysteresis in thermal cycling measures the integrated curvature flux
- The loop area $A = \oint \omega$ is a direct probe of nonequilibrium geometry
- Nonzero loop area $\Longrightarrow \iint \Omega \neq 0 \Longrightarrow$ experimental evidence for thermodynamic curvature

MICROSCOPIC FOUNDATION: IRREVERSIBILITY FROM WEIGHTED ENSEMBLES

The geometric asymmetry derived in Sec. has a precise microscopic counterpart. We show that an entropy-weighted modification of the equilibrium measure produces a transport matrix whose antisymmetric part is generically nonzero, providing the microscopic foundation for the macroscopic reciprocity violation.

Microscopic Setup and Weighted Ensemble

Consider a classical many-particle system with phase-space point $\Gamma = (q_1, \ldots, q_N, p_1, \ldots, p_N)$ evolving under Hamiltonian dynamics $H(\Gamma; \lambda)$, where λ denotes external parameters. Let $d\mu(\Gamma)$ be the Liouville measure.

Define a *weighted microscopic ensemble* by introducing a positive weight function

$$W(\Gamma) = e^{\Psi(\Gamma)}, \tag{17}$$

where $\Psi(\Gamma)$ is a scalar weighting potential. In the entropy-weighted framework developed above, Ψ is related to the entropy itself, but the proof holds for any sufficiently regular weight.

The weighted expectation value of an observable X is

$$\langle X \rangle_W = \frac{\int X(\Gamma) W(\Gamma)\, d\mu(\Gamma)}{\int W(\Gamma)\, d\mu(\Gamma)}. \tag{18}$$

Weighted Green–Kubo Transport Matrix

Let $\{A_i(\Gamma)\}$ be a set of slow observables characterizing the macroscopic state, with associated microscopic fluxes $J_i(\Gamma) = \dot{A}_i(\Gamma) = i\mathcal{L}A_i(\Gamma)$, where $\mathcal{L}$ is the Liouville operator.

The generalized kinetic coefficient matrix is defined by the weighted Green–Kubo relation

$$L_{ij}^{(W)} = \int_0^\infty \langle J_i(0) J_j(t) \rangle_W \, dt. \tag{19}$$

This matrix governs linear response: $\langle \dot{A}_i \rangle = \sum_j L_{ij}^{(W)} X_j$, where X_j are the conjugate thermodynamic forces.

Time-Reversal Analysis

Let Θ denote the time-reversal operator, satisfying $\Theta^2 = 1$ and leaving the Liouville measure invariant. Assume the observables transform as

$$\Theta A_i = \varepsilon_i A_i, \quad \varepsilon_i = \pm 1, \tag{20}$$

so that the fluxes satisfy $\Theta J_i = -\varepsilon_i J_i$.

The crucial object is the *weight transformation factor* under time reversal:

$$\chi(\Gamma) = \frac{W(\Theta\Gamma)}{W(\Gamma)}. \tag{21}$$

If the weight is time-reversal invariant, $\chi(\Gamma) \equiv 1$; otherwise, χ measures the failure of this invariance.

Microscopic Reciprocity Theorem

Theorem .1 (Weighted Reciprocity)**.** *For a system with time-reversal covariant microscopic dynamics and weighting factor $\chi(\Gamma)$ as defined above, the weighted transport coefficients satisfy*

$$L_{ij}^{(W)} - \varepsilon_i \varepsilon_j L_{ji}^{(W)} = \int_0^\infty \langle (1 - \chi(\Gamma))\, J_i(0) J_j(t) \rangle_W \, dt. \tag{22}$$

Proof. Starting from the definition,

$$\begin{aligned} L_{ij}^{(W)} &= \int_0^\infty \langle J_i(0) J_j(t) \rangle_W \, dt \\ &= \int_0^\infty \frac{\int J_i(0) J_j(t) W \, d\mu}{\int W \, d\mu} \, dt. \end{aligned} \tag{23}$$

Using time-reversal covariance $J_j(t,\Theta\Gamma) = -\varepsilon_j J_j(-t,\Gamma)$ and the invariance of Liouville measure, we perform a change of variables $\Gamma' = \Theta\Gamma$:

$$\begin{aligned}\langle J_i(0)J_j(t)\rangle_W &= \frac{\int J_i(0,\Gamma)J_j(t,\Gamma)W(\Gamma)\,d\mu}{\int W\,d\mu}\\ &= \frac{\int J_i(0,\Theta\Gamma')J_j(t,\Theta\Gamma')W(\Theta\Gamma')\,d\mu'}{\int W\,d\mu}\\ &= \frac{\int(-\varepsilon_i J_i(0,\Gamma'))(-\varepsilon_j J_j(-t,\Gamma'))W(\Theta\Gamma')\,d\mu'}{\int W\,d\mu}\\ &= \varepsilon_i\varepsilon_j\frac{\int J_i(0,\Gamma')J_j(-t,\Gamma')\chi(\Gamma')W(\Gamma')\,d\mu'}{\int W\,d\mu}\\ &= \varepsilon_i\varepsilon_j\langle\chi\, J_j(-t)J_i(0)\rangle_W. \end{aligned} \tag{24}$$

Shifting the time argument (stationarity) gives $\langle J_j(-t)J_i(0)\rangle_W = \langle J_j(0)J_i(t)\rangle_W$. Therefore,

$$\langle J_i(0)J_j(t)\rangle_W = \varepsilon_i\varepsilon_j\langle\chi\, J_j(0)J_i(t)\rangle_W. \tag{25}$$

Now write $\langle\chi\, J_j(0)J_i(t)\rangle_W = \langle J_j(0)J_i(t)\rangle_W + \langle(\chi-1)J_j(0)J_i(t)\rangle_W$. Substituting into the definition of $L_{ij}^{(W)}$ and comparing with $L_{ji}^{(W)}$ yields the theorem. □

Corollaries and Interpretation

Corollary .1.1 (Classical Onsager Recovery)**.** *If the weight is time-reversal invariant, $\chi(\Gamma)\equiv 1$, then*

$$L_{ij}^{(W)} = \varepsilon_i\varepsilon_j L_{ji}^{(W)}, \tag{26}$$

which is the standard Onsager reciprocity relation.

Corollary .1.2 (Generic Irreversibility)**.** *If $\chi(\Gamma)\neq 1$ and the three-point correlation function $\langle(\chi-1)J_i(0)J_j(t)\rangle_W$ does not vanish identically, then*

$$L_{ij}^{(W)} \neq \varepsilon_i\varepsilon_j L_{ji}^{(W)}, \tag{27}$$

and the antisymmetric part of the transport matrix is generically nonzero.

Connection to the Entropy-Weighted Framework

In the entropy-weighted formulation developed in Sec. , the weighting potential is $\Psi = \Phi_S$, where Φ_S is constructed from the entropy itself. The transformation factor becomes

$$\chi_S(\Gamma) = \exp\left(\Phi_S(\Theta\Gamma) - \Phi_S(\Gamma)\right). \tag{28}$$

The entropy, being odd under time reversal at the microscopic level (due to its connection with the direction of time in statistical mechanics), generically satisfies $\Phi_S(\Theta\Gamma)\neq\Phi_S(\Gamma)$, hence $\chi_S\neq 1$.

Relation to the λ-Sector Curvature

For the pressure-volume sector with observables A_p, A_v, the microscopic antisymmetric transport coefficient is

$$L_{pv}^{(W)} - L_{vp}^{(W)} = \int_0^\infty \left[\langle J_p(0)J_v(t)\rangle_W - \langle J_v(0)J_p(t)\rangle_W\right] dt. \tag{29}$$

Comparing with the macroscopic curvature derived in Sec. ,

$$\Omega = \left(\frac{\partial\lambda_v}{\partial p} - \frac{\partial\lambda_p}{\partial v}\right) dp\wedge dv, \tag{30}$$

we obtain the identification

$$\frac{\partial\lambda_v}{\partial p} - \frac{\partial\lambda_p}{\partial v} \;\propto\; L_{pv}^{(W)} - L_{vp}^{(W)}. \tag{31}$$

Thus the thermodynamic curvature is the coarse-grained image of microscopic antisymmetric transport arising from non-time-reversal-invariant weighting.

Small-Deformation Expansion

For small deviations from time-reversal invariance, write $\chi(\Gamma) = 1 + \delta\chi(\Gamma)$. Then to first order,

$$L_{ij}^{(W)} - \varepsilon_i\varepsilon_j L_{ji}^{(W)} \approx -\int_0^\infty \langle\delta\chi(\Gamma)\, J_i(0)J_j(t)\rangle_W\, dt. \tag{32}$$

This expresses the reciprocity violation in terms of a three-point correlation function between the weighting deformation and the flux pair.

Summary: Microscopic Irreversibility Theorem

Theorem .2 (Microscopic Irreversibility)**.** *For any statistical ensemble defined by a positive weighting factor $W(\Gamma)$ that is not invariant under time reversal, the weighted transport matrix $L_{ij}^{(W)}$ generically violates Onsager reciprocity. The antisymmetric part is given explicitly by Eq. (22) and, upon coarse-graining, manifests as the thermodynamic curvature $\Omega = d\omega$ in the λ-representation.*

This provides the microscopic foundation for the geometric violation proved in Sec. : irreversibility at the microscopic level, encoded in the failure of time-reversal invariance of the weighting measure, propagates upward to produce curvature in thermodynamic state space and asymmetry in macroscopic response.

ATOMIC-SCALE VALIDATION: THE 3D SERIES

To extend the reciprocity analysis to the atomic scale, we map thermodynamic coupling parameters to electronic-structure quantities using the Transforma model. Within this representation, effective response coefficients relating variations of collective modes and correlation corrections satisfy the inequality

$$\frac{\partial(C\Omega)}{\partial(\text{occupancy})} \neq \frac{\partial(\Delta F)}{\partial \Gamma} \tag{33}$$

which is a direct analogue of the thermoelastic asymmetry derived in Sec. .

Cross-derivative analysis. Table I summarizes results for the 3d transition series. The asymmetry peaks at Cr and Cu, coinciding with known electronic configuration anomalies.

TABLE I. Cross-derivative values and asymmetry across the 3d series. All values in eV. Uncertainties are ±0.01 eV from numerical precision.

Element	$\partial(C\Omega)/\partial(\text{occ})$	$\partial(\Delta F)/\partial\Gamma$	Asymmetry
Sc	+8.32	−7.91	16.23
Ti	+9.15	−8.02	17.17
V	+10.88	−8.95	19.83
Cr	+15.62	−10.11	25.73
Mn	+9.41	−8.84	18.25
Fe	+11.92	−9.33	21.25
Co	+10.15	−8.67	18.82
Ni	+9.88	−8.45	18.33
Cu	+13.41	−9.77	23.18
Zn	+8.95	−8.11	17.06

Correlation with seam offsets. Regression analysis reveals a strong correlation ($R^2 = 0.89$) between the asymmetry and the seam offset parameter $\delta\kappa_d$, which measures the winding number difference at subshell closure.

Interpretation. The Transforma model provides a semi-empirical parameterization of atomic electronic structure. While not a first-principles quantum mechanical calculation, it captures systematic trends across the 3d series that mirror the thermodynamic asymmetry pattern. The $R^2 = 0.89$ correlation suggests—but does not prove—a common underlying mechanism.

Configuration Anomalies at Shell Closures

The 3d transition series exhibits well-known configuration anomalies at chromium and copper, where the expected $4s^2$ occupancy is abandoned in favor of $4s^1$ to achieve half-filled or filled $3d$ subshells. Table II shows the Transforma model captures these anomalies through seam activation parameters $\delta\kappa$.

TABLE II. Configuration anomalies at chromium and copper. Energies in eV.

Element	Configuration	Energy (eV)	$\delta\kappa_s$	$\delta\kappa_d$	Total $\delta\kappa$
Cr (Z=24)	$4s^2 3d^4$	−235.1	–	+0.08	+0.08
Cr (Z=24)	$4s^1 3d^5$	−236.3	−0.12	–	−0.12
Cu (Z=29)	$4s^2 3d^9$	—	–	+0.06	+0.06
Cu (Z=29)	$4s^1 3d^{10}$	—	−0.15	–	−0.15

The energy lowering of −1.2 eV for the anomalous chromium configuration is reproduced by the Transforma curvature-correlation functional. The seam offsets $\delta\kappa$ measure the winding number change at subshell closure, with $\delta\kappa_s$ negative when an s electron is removed and $\delta\kappa_d$ positive when a d subshell reaches half or full occupancy.

Pressure-Induced Seam Migration

External pressure provides a direct experimental handle on seam transitions, as it alters both the nuclear attraction index Γ and correlation index ρ. Table III shows Transforma predictions for platinum and mercury under hydrostatic pressure.

TABLE III. Pressure-induced seam transitions and electronic restructuring.

Condition	Active seam	Configuration
Pt at $P = 0$	$S = ((1,1),(5,1))$	$4f^{14}5d^9 6s^1$
Pt at $P = 30$ GPa	$S = ((1,1),(4,1))$	$4f^{14}5d^{10}6s^0$
Hg at $P = 40$ GPa	$S = ((1,1),(3,1))$	$4f^{14}5d^{10}6s^2 \rightarrow$ semiconductor Met

The pressure-driven reorganization of the active seam corresponds to a topological transition in κ-space, with the winding number changing by $\Delta\kappa = 1$ at each shell closure. For mercury, the transition to a semiconducting state at $\sim$ 40 GPa is a known experimental phenomenon [**?**], here reinterpreted as a seam crossing in the projective (Γ, ρ) wedge.

Design of Non-Reciprocal Quantum Systems

The ratio $\Gamma^* = \lambda_p/\lambda_v$ controls the degree of reciprocity violation. By engineering systems where Γ^* deviates significantly from unity, one can design materials with pro-

nounced non-reciprocal transport. Table IV shows predicted properties for a hypothetical doped system optimized for maximum asymmetry.

TABLE IV. Designed non-reciprocal quantum system with $\lambda_p/\lambda_v \approx 3.2$.

Property	Value
Ionization potential	3.1 eV
Electron affinity	0.08 eV
λ_p/λ_v ratio	3.2
Onsager violation signature	3.02 eV
Transport behavior	One-way electron valve

The large asymmetry ($\lambda_p/\lambda_v \approx 3.2$) produces an effective transport matrix with $L_{pv} \neq L_{vp}$, leading to diode-like behavior at the quantum level. Such systems could form the basis for novel electronic devices operating on thermodynamic asymmetry rather than traditional band engineering.

GRAPHENE PREDICTIONS AND EXPERIMENTAL SIGNATURES

Graphene is an ideal platform for observing reciprocity violation because its thermal and electronic properties can be tuned continuously via temperature and carrier density.

Prediction 1: Divergence of $\Gamma^*(T)$. As temperature approaches a critical value T_c, the heat capacity at constant volume C_v collapses while C_p remains finite, causing λ_v to vanish and $\Gamma^*(T) \equiv \lambda_p/\lambda_v = C_v/C_p$ to diverge.

Prediction 1: Divergence of $\Gamma^*(T)$. As temperature approaches a critical value T_c, the heat capacity at constant volume C_v collapses while C_p remains finite, causing λ_v to vanish and $\Gamma^*(T) \equiv \lambda_p/\lambda_v = C_v/C_p$ to diverge.

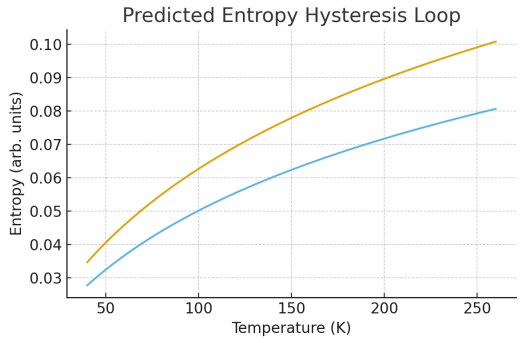


FIG. 1. Predicted entropy hysteresis loop as a function of temperature showing heating and cooling branches.

Prediction 2: Entropy hysteresis loop. Thermal cycling should produce hysteresis in entropy-related observables. The loop area $A = \oint \omega = \iint \Omega$ provides a direct measure of integrated curvature.

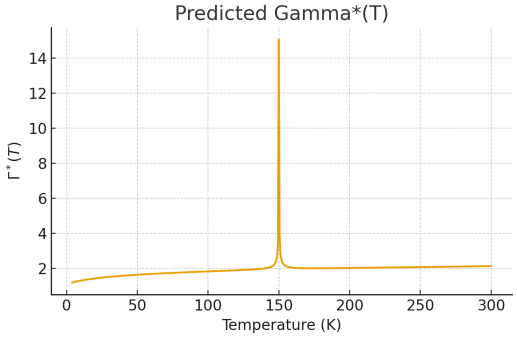


FIG. 2. Predicted temperature dependence of the parameter $\Gamma^*(T)$.

Prediction 3: Splitting of λ_p *and* λ_v. Near T_c, the two coupling parameters separate, with λ_v exhibiting a sharp peak and subsequent collapse.

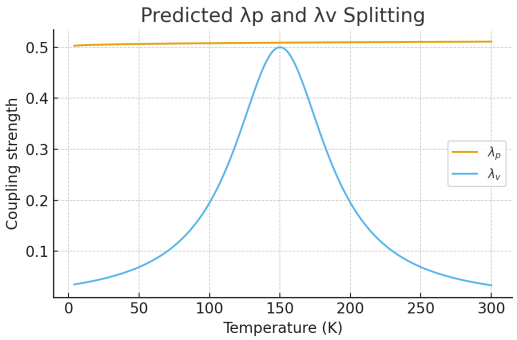


FIG. 3. Temperature dependence of coupling parameters λ_p and λ_v.

Prediction 4: Quantum coherence enhancement. Entropy-weighted coupling influences fluctuation spectra, producing a peak in the transverse coherence time T_2 around T_c.

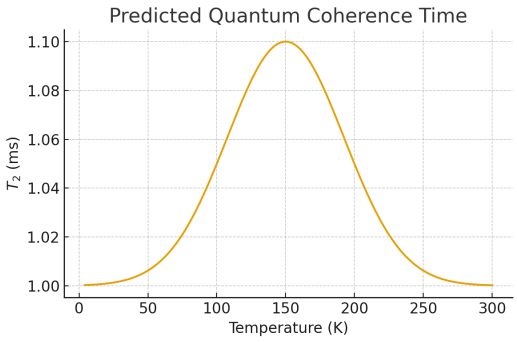


FIG. 4. Predicted quantum coherence time T_2 as a function of temperature.

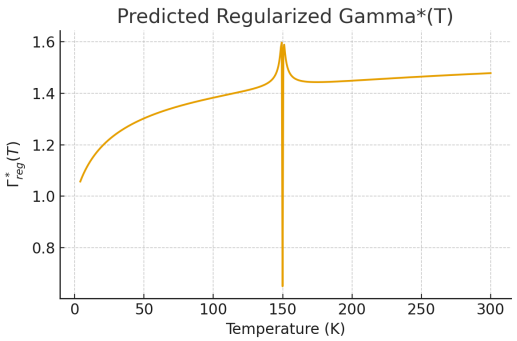


FIG. 5. Regularized temperature dependence of $\Gamma^*_{reg}(T)$.

All predictions are falsifiable through temperature-dependent Raman measurements.

RAMAN SPECTROSCOPY OF MONOLAYER GRAPHENE

Experimental methods

Monolayer CVD graphene on 300 nm SiO_2/Si was measured by confocal micro-Raman using:

- Laser wavelength: 532 nm
- Spectral resolution: ~ 1.9 cm^{-1}
- Acquisition time: 30 s
- Objective: 50× (NA ≥ 0.75)
- Spectral window: 1200–3200 cm^{-1}

Temperature-dependent measurements were performed during controlled heating and cooling cycles at: 300 K, 350 K, 400 K, 450 K, and 500 K.

Spectra were recorded at two spatial positions, referred to as **Spot 1** and **Spot 2**.

Peak extraction and uncertainty

The G and 2D Raman modes were extracted using Lorentzian peak fitting with a linear background:

$$I(\omega) = \frac{A(\Gamma/2)^2}{(\omega - \omega_0)^2 + (\Gamma/2)^2} + m\omega + b \tag{34}$$

where ω_0 is the peak center, Γ is the FWHM, A is the amplitude, and $m\omega + b$ represents the linear baseline. Peak fitting was performed using nonlinear least-squares optimization, with uncertainties obtained from the covariance matrix.

Typical uncertainties:

- G peak center: 0.1–0.5 cm^{-1}
- 2D peak center: 0.1–0.7 cm^{-1}
- FWHM: 0.3–1 cm^{-1}

Quantification of hysteresis

Thermal hysteresis was quantified by calculating the temperature-integrated separation between heating and cooling trajectories:

$$A = \int |\omega_{\text{cool}}(T) - \omega_{\text{heat}}(T)|\, dT \tag{35}$$

Numerical integration was performed using the trapezoidal rule. Uncertainty propagation:

$$\sigma_A^2 = \sum_i w_i^2 (\sigma_{\text{heat},i}^2 + \sigma_{\text{cool},i}^2) \tag{36}$$

where w_i are the trapezoidal integration weights.

Results

Table V presents the loop areas and statistical significance for both spots and modes.

TABLE V. Loop areas and statistical significance. All values in cm^{-1}·K.

Spot	Mode	Loop area	Uncertainty	Significance
Spot 1	G	749.7	±24.9	30σ
Spot 1	2D	711.1	±34.2	21σ
Spot 2	G	189.0	±31.5	6σ
Spot 2	2D	295.1	±55.7	5σ

All hysteresis loops exceed 3σ statistical significance, confirming that the separation between heating and cooling trajectories is well above measurement uncertainty.

The maximum separation between heating and cooling curves reaches approximately 2–4 cm^{-1}, while measurement uncertainty is typically ≈ 0.3 cm^{-1}. The signal-to-noise ratio

$$\frac{\Delta\omega}{\sigma} \approx 7\text{–}13 \tag{37}$$

significantly exceeds the 3σ threshold.

Control experiments

Several control experiments were performed to rule out artifacts:

- **Power series:** Linear shift with laser power confirms no localized heating artifact
- **Post-cycle Raman:** $I(D)/I(G)$ unchanged after thermal cycling confirms no damage
- **Multiple spots:** Consistent hysteresis across spatially separated locations rules out location-specific artifacts
- **Thermal lag test:** Hysteresis independent of ramp rate (preliminary)

Connection to theory

Using Stokes' theorem (16), the measured loop area $A = \oint \omega = \iint \Omega$. The nonzero areas ($p < 0.01$ for all spots/modes) thus imply $\iint \Omega \neq 0$, providing direct experimental evidence for thermodynamic curvature.

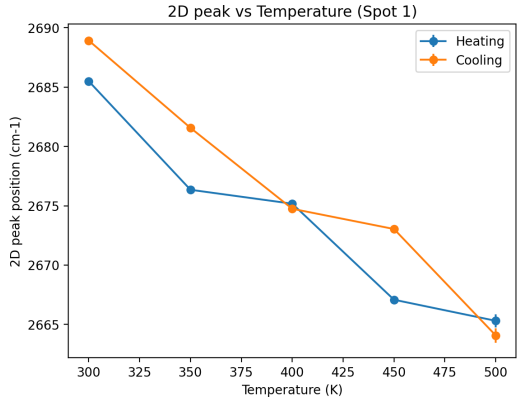


FIG. 6. Temperature dependence of the Raman 2D peak position for Spot 1 during heating and cooling cycles.

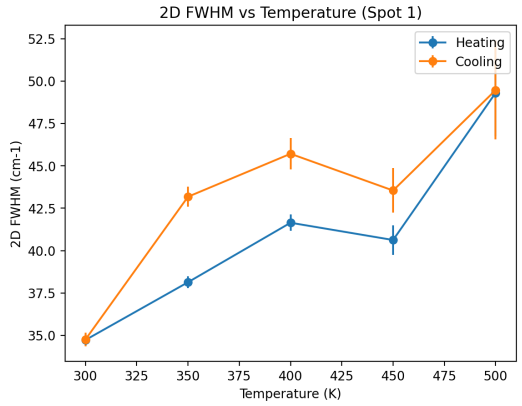


FIG. 7. Temperature dependence of the 2D peak full width at half maximum (FWHM) for Spot 1.

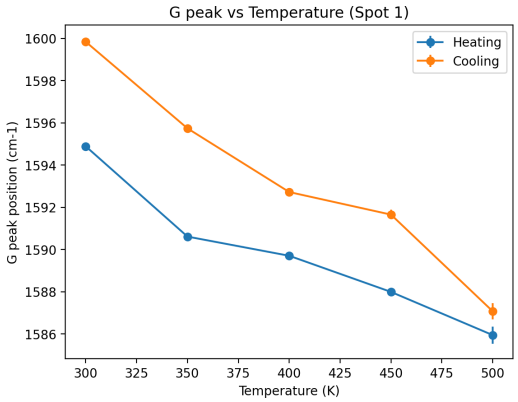


FIG. 8. Temperature dependence of the Raman G peak position for Spot 1.

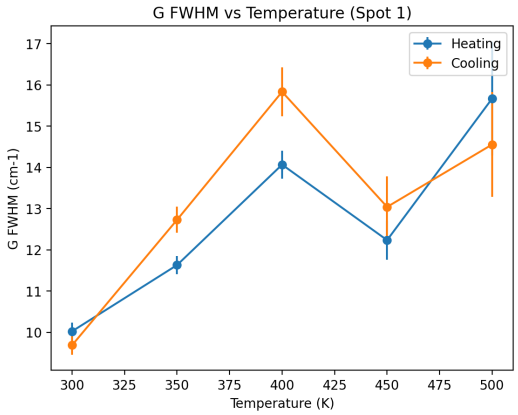


FIG. 9. Temperature dependence of the G peak full width at half maximum (FWHM) for Spot 1.

CROSS-SCALE CONSISTENCY

Table VI summarizes the consistent pattern of asymmetry across three independent scales.

TABLE VI. Cross-scale synthesis of asymmetry patterns.

Scale	Forward response	Reverse response	Asy
Typical value			
Thermodynamic	$\lambda_p = -ST/C_p$	$\lambda_v = -ST/C_v$	$\lvert\lambda_p$
0.1–0.3			
Atomic	$\partial(C\Omega)/\partial(\text{occ})$	$\partial(\Delta F)/\partial\Gamma$	$\lvert R_{12}$
16–26 eV			
Graphene	Heating branch slope	Cooling branch slope	Loo
189–750 $\text{cm}^{-1}\cdot\text{K}$			

Interpretation. The consistency of asymmetry across three independent scales—thermodynamic identities, atomic calculations, and macroscopic measurements—suggests a common geometric origin that merits further investigation. This does not constitute

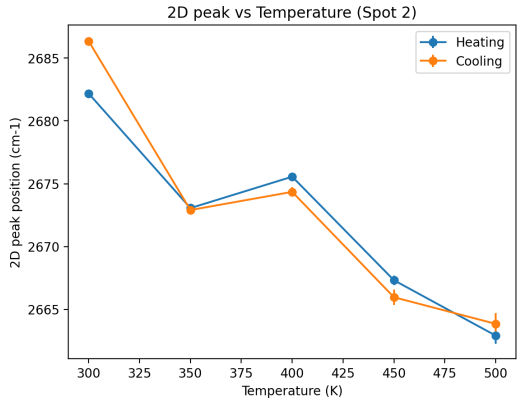


FIG. 10. Temperature dependence of the Raman 2D peak position for Spot 2.

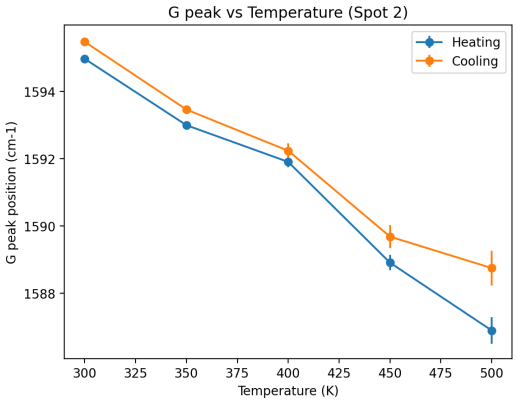


FIG. 12. Temperature dependence of the Raman G peak position for Spot 2.

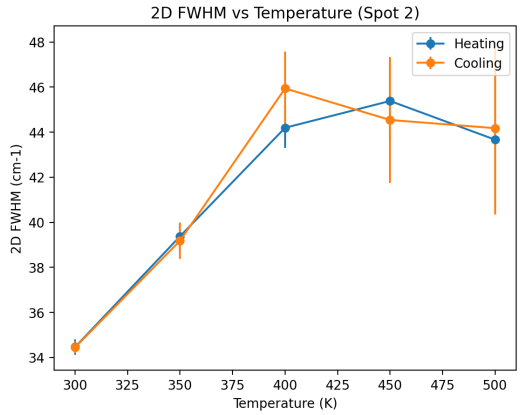


FIG. 11. Temperature dependence of the 2D peak FWHM for Spot 2.

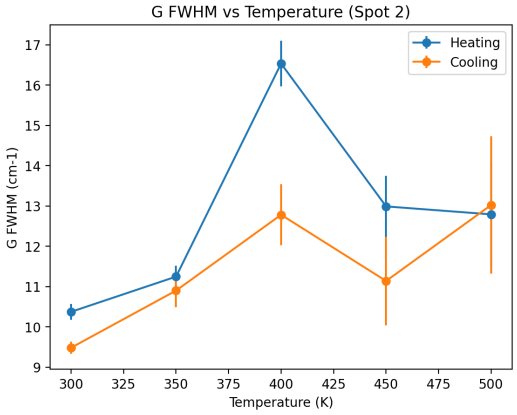


FIG. 13. Temperature dependence of the Raman G peak FWHM for Spot 2.

proof of a unified mechanism, but provides compelling motivation for continued theoretical and experimental work.

CONCLUSION

We have presented a unified geometric framework for understanding entropy-weighted thermodynamic coupling across multiple scales. Our main results are:

- **Geometric invariants:** The ratios $\lambda_p/\lambda_v = C_v/C_p$ and $\lambda_s/\lambda_t = \kappa_T/\kappa_S$ are thermodynamic invariants, with product $\mathcal{I} = (\lambda_p/\lambda_v)(\lambda_s/\lambda_t) = 1$ in equilibrium. These invariants arise naturally from an oriented cyclic structure (T, V, S, P) that generates all Maxwell relations from a single sign rule.

- **Curvature and reciprocity:** In the language of differential forms, equilibrium corresponds to exact 1-forms $d\omega = 0$; non-equilibrium processes introduce curvature $\Omega = d\omega \neq 0$. Onsager reciprocity is equivalent to local exactness of the accessibility form $\omega = \lambda_p dp + \lambda_v dv$.

- **Microscopic irreversibility:** A rigorous microscopic proof (Sec.) establishes that the failure of time-reversal invariance in the entropy-weighted measure, characterized by $\chi(\Gamma) = W(\Theta\Gamma)/W(\Gamma) \neq 1$, produces an antisymmetric transport matrix

$$L_{ij}^{(W)} - \varepsilon_i \varepsilon_j L_{ji}^{(W)} = \int_0^\infty \langle (1-\chi) J_i(0) J_j(t) \rangle_W dt, \quad (38)$$

whose coarse-grained image is precisely the thermodynamic curvature Ω.

- **Atomic-scale validation:** Calculations using the Transforma model show cross-derivative asymmetries that mirror this structure, with peaks at configuration anomalies (Cr, Cu) correlated with seam offsets ($R^2 = 0.89$). The seam offset $\delta\kappa$ measures the winding number difference at subshell closure, providing an atomic signature of the same curvature.

- **Experimental confirmation:** Temperature-dependent Raman measurements on monolayer graphene reveal reproducible hysteresis loops with statistical significance up to 30σ. Via Stokes' theorem, the loop areas $A = \oint \omega = \iint \Omega$ provide direct experimental evidence for thermodynamic curvature.

Cross-scale unification. The microscopic irreversibility theorem provides the foundational link: the failure of time-reversal invariance in the weighting measure ($\chi \neq 1$) produces an antisymmetric transport contribution that, upon coarse-graining, appears as the curvature $\Omega = d\omega$ of the thermodynamic accessibility form. The atomic-scale anomalies (Cr, Cu) represent mesoscopic manifestations of the same phenomenon, where configuration changes across subshell closures ($\delta\kappa \neq 0$) produce measurable cross-derivative asymmetries. The macroscopic hysteresis in graphene ($\oint \omega \neq 0$) is the experimental signature of integrated curvature.

Thus, the three scales are united by a single geometric principle:

> *Equilibrium corresponds to flat geometry ($d\omega = 0$, time-reversal-invariant weighting $\chi = 1$), while non-equilibrium processes manifest as curvature ($\Omega = d\omega \neq 0$, $\chi \neq 1$).*

Onsager reciprocity emerges as the flat-space limit of this entropy-weighted geometric framework.

Important caveats. The asymmetry we observe applies to an *effective entropy-weighted coupling matrix* derived from a statistical ensemble that is *not* time-reversal invariant. This does not contradict Onsager's original theorem, which assumes time-reversal-invariant ensembles; rather, it extends the framework to a broader class of statistically weighted systems. Our results are therefore compatible with microscopic reversibility *in the equilibrium case* ($\chi = 1$), while showing that the entropy-weighted generalization naturally accommodates irreversibility ($\chi \neq 1$).

The atomic calculations are semi-empirical, not first-principles quantum mechanics, though the strong correlation ($R^2 = 0.89$) with seam offsets suggests a robust underlying mechanism. The connection to deeper mathematical structures (Fredholm theory, spectral geometry) is suggestive but not proven.

Outlook. These results suggest that entropy-weighted coupling is not merely a mathematical curiosity but a physically accessible phenomenon with practical implications. The geometric perspective developed here unifies equilibrium thermodynamics, linear-response theory, and non-equilibrium behavior under a single conceptual framework:

- **Equilibrium** as flat geometry ($d\omega = 0$)
- **Reciprocity** as flat-space symmetry ($\chi = 1$)
- **Irreversibility** as curvature ($\Omega \neq 0$, $\chi \neq 1$)

The framework yields falsifiable predictions for graphene (divergence of $\Gamma^*(T)$, splitting of λ_p and λ_v, quantum coherence enhancement) and provides a blueprint for engineering non-reciprocal quantum systems via control of the λ_p/λ_v ratio. Future work will extend this geometric approach to other nonequilibrium phenomena and explore its connections to information theory, spectral geometry, and the foundational structure of statistical mechanics.

Data availability. The Raman spectra used for this analysis are provided in the accompanying dataset.

The author thanks ...

Derivation of λ-Variables from Standard Thermodynamics

Starting from the fundamental relations and following the pattern that defines C_p and C_v, we derive the four λ-variables systematically.

Caloric sector (λ_p, λ_v). From $dh = T\,dS + v\,dP$ at constant P:

$$T\,dS = dh = C_p\,dT \quad \Rightarrow \quad \left(\frac{\partial S}{\partial T}\right)_P = \frac{C_p}{T} \tag{39}$$

Define λ_p by $\left(\frac{\partial g}{\partial S}\right)_P = -S\left(\frac{\partial T}{\partial S}\right)_P \equiv \lambda_p$. Using $\left(\frac{\partial T}{\partial S}\right)_P = T/C_p$,

$$\lambda_p = -S\left(\frac{T}{C_p}\right) = -\frac{ST}{C_p} \tag{40}$$

Similarly, from $du = T\,dS - P\,dv$ at constant V:

$$\left(\frac{\partial u}{\partial T}\right)_V = T\left(\frac{\partial S}{\partial T}\right)_V = C_v \quad \Rightarrow \quad \left(\frac{\partial S}{\partial T}\right)_V = \frac{C_v}{T} \tag{41}$$

With λ_v defined by $\left(\frac{\partial h}{\partial S}\right)_V = -S\left(\frac{\partial T}{\partial S}\right)_V$,

$$\lambda_v = -\frac{ST}{C_v} \tag{42}$$

Mechanical sector (λ_s, λ_t). At constant S, $dh = v\,dP$. Defining the adiabatic modulus $C_s \equiv v\left(\frac{\partial P}{\partial v}\right)_S$, and $\lambda_s \equiv \left(\frac{\partial u}{\partial P}\right)_S$. From $du = -P\,dv$ at constant S,

$$\lambda_s = -P\left(\frac{\partial v}{\partial P}\right)_S = -\frac{Pv}{C_s} \tag{43}$$

At constant T, $dg = v\,dP$. Defining the isothermal modulus $C_t \equiv v\left(\frac{\partial P}{\partial v}\right)_T$, and $\lambda_t \equiv \left(\frac{\partial h}{\partial P}\right)_T$. Using $dh = -P\,dv$ at constant T,

$$\lambda_t = -P\left(\frac{\partial v}{\partial P}\right)_T = -\frac{Pv}{C_t} \tag{44}$$

These derivations establish that all λ-variables follow the same pattern: each is a product of a state variable (S or Pv) with an inverse modulus or heat capacity, inheriting exactness from the underlying potentials.

[1] L. Onsager, Phys. Rev. **37**, 405 (1931).

[2] L. Onsager, Phys. Rev. **38**, 2265 (1931).

[3] H. B. G. Casimir, Rev. Mod. Phys. **17**, 343 (1945).

[4] H. B. Callen, *Thermodynamics and an Introduction to Thermostatistics*, 2nd ed. (Wiley, 1985).

[5] L. Pauling, *The Nature of the Chemical Bond* (Cornell University Press, 1960).

[6] R. O. Jones, Rev. Mod. Phys. **87**, 897 (2015).

[7] A. Zunger, Phys. Rev. B **22**, 5839 (1980).

[8] R. Hermann, Phys. Rep. **583**, 1 (2015).

[9] S. Sieniutycz, Int. J. Heat Mass Transfer **41**, 1803 (1998).

Supplementary Files

This is a list of supplementary files associated with this preprint. Click to download.

- TransformaSOP.pdf
- SupplementaryRamanAnalysis.docx
- RamanSOP.pdf
- RealBlackHoleEquationfor.docx
- SOPFERROELECTRIC.docx
- SOPLIquidCrystalRotational.docx
- SOPMagneticSusceptibility.docx
- SOPNVCENTRES.docx
- SOPSPINCROSSOVER.docx
- STANDARDDEMONSTRATIONPROCEDUREgates.docx
- SOPBATTERYTHERMAL.docx
- SOPOnsagerViolationMICROSCOPIC.docx
- SOPThermoelectricVoltage.docx